RSC Advances

ROYAL SOCIETY OF CHEMISTRY

www.rsc.org/advances

RSC Advances

RSCPublishing

ARTICLE

The Structure, Carbon Deposition and Stability of a ZrO_x/Ni-MnO_x/SiO_2 Catalyst for the CO_2 Reforming of Methane†

Lu Yao, Jia Shi and Changwei Hu*

Cite this: DOI: 10.1039/xoxxoooooox

Received ooth January 2012,
Accepted ooth January 2012

DOI: 10.1039/xoxxoooooox

www.rsc.org/

A Zr and Mn co-promoted Ni-based catalyst was prepared using impregnation method and employed for the dry reforming of methane. Characterization of the catalysts has been performed using XRD, TEM Mapping, XPS, TPR, TPO, TG, TPH and Raman techniques. The results showed that the addition sequence of the Mn and Zr promoters contributed substantially to the structure and activity of the catalyst. A high dispersion of the Ni, Mn and Zr species and strong interactions of the metallic oxides with support were observed on ZrO_X/Ni-MnO_X/SiO_2 catalyst, which enhanced the formation of polymeric carbon species capable of being gasified by CO_2 to release CO and H_2. Under these conditions the ZrO_X/Ni-MnO_X/SiO_2 catalyst exhibited high initial activity and excellent stability.

1 Introduction

CO_2 reforming of CH_4 (dry reforming of methane, DRM) appears to be attractive because of its capacity to mitigate climate change through the transformation of two greenhouse gases (CH_4 and CO_2) into synthesis gas, a mixture of H_2 and CO, which is the basis of Fischer-Tropsch chemistry.[1-5] Besides, biomass derived gas mixture generally has a high content of CO_2 and CH_4, thus, DRM process also attracted much attention due to increased interest in utilizing biomass derived gaseous products.[2] Moreover, the efficient upgrading of methane has been a longstanding challenge for the scientific community because CH_4 exhibits a high C-H bond strength (434 kJ/mol).[6-8]

Ni-based catalysts have been regarded as the most promising candidates because of their low cost and extensive supply.[1,9-14] However, poor stability caused by carbon deposition and sintering of active Ni metal limits the industrial application of Ni catalysts in the DRM reaction.[1,9-17] Prevention of the deactivation of Ni catalysts still remains a challenge.[14-17] Thus, there is a need to develop catalysts capable of resisting deactivation by sintering and carbon formation, because a balance between the formation and oxidation of surface carbon is necessary for the stability of the DRM catalyst. For example, Li and co-workers have doped Mg into Ni@SiO_2 catalyst to form Ni@Ni-Mg silicate core shell catalyst, which showed quite good catalytic performance for DRM reaction with stable and high CO_2 and CH_4 conversions within 95 h reaction duration at 700 ° C.[18] There are several ways to increase deactivation resistance, such as increasing and maintaining the dispersion of the active metal [14,19-21] and improving the oxidation rate of the surface carbon.[20-22]

The introduction of a second (or several) metal(s) is a recognized way to improve the stability and catalytic activity of Ni-based catalysts.[23-25]

Sutthiumporn et. al. studied the promotional effect of alkaline earth over Ni-La_2O_3 catalyst for DRM process.[24] They found that the Sr-promoted Ni-La_2O_3 catalyst yielded the highest catalytic activity and lowest carbon deposition. Besides, they also developed the $La_{0.8}Sr_{0.2}Ni_{0.8}M_{0.2}O_3$ (LSNMO) (where M = Bi, Co, Cr, Cu and Fe) perovskite catalyst precursors for DRM process.[25] They reported that LSN(Cu)O perovskite possessed good initial activity, whereas LSN(Fe)O perovskite showed high final activity and stability with no formation of deposited carbon.

In addition to the promoters mentioned above, Zr or Mn was also one of the candidate metals. [26-28]

A reasonably high activity for the DRM reaction was obtained using the Ni/$La_2Zr_2O_7$ catalyst by Ma and co-workers.[26] They found that a large amount of $La_2O_2CO_3$ was formed on the spent Ni/$La_2Zr_2O_7$ catalyst, and these species reacted with the deposited carbon formed on the Ni particles and continuously restored the Ni sites. Thus, they suggested that as coking was suppressed and the high initial activity of the catalyst was maintained, the Ni/$La_2Zr_2O_7$ catalyst was a superior catalyst with the potential for industrial use.

Liu and co-workers found that all Zr-promoted catalysts exhibited comparable or enhanced initial catalytic activity compared with that of Ni-MCM-41.[27] They suggested that the strong anchoring effect of Zr^{4+} and the partial activation of CO_2 by Zr^{4+} contributed to the high catalytic activity.

A γ-Al_2O_3 support modified with ZrO_2 by a grafting method was employed by Fernández and co-workers.[28] They found a significant improvement in the catalytic performance with the grafted catalyst, which was apparently formed by Rh/γ-Al_2O_3 and Rh/ZrO_2 particles in physical contact. The mixtures with a low content of Rh/ZrO_2 catalyst exhibited a higher activity compared with the single catalyst, and an important synergistic effect was observed. They suggested that this cooperative effect was magnified in the grafted sample,

which presented a large number of high-quality contacts between Rh/γ-Al_2O_3 and Rh/ZrO_2.

Seok and co-workers reported that the addition of Mn to Ni/Al_2O_3 facilitated the adsorption of CO_2 by reforming a reactive carbonate species, and the contiguous surface Ni was partly blocked ("decorated") by patches of MnO_x.[29] Both of these effects appeared to be responsible for the suppression of carbon deposition over the Ni/MnO-Al_2O_3 catalyst, which improved the ability of the catalyst in the DRM reaction.

In our previous work, the Ni/SiO_2 catalysts promoted by Zr or Mn were investigated comparatively.[30] We found that the introduction of Mn promoted the dispersion of the Ni species, which enabled the catalyst to minimize carbon deposition and yet exhibit good stability within the reaction temperature range tested (800, 750, 700, 650 and 600 °C). The introduction of Zr considerably enhanced the initial catalytic activity, but an obvious deactivation of the catalyst was observed during the 60 h DRM reaction.

We devoted this paper to integrating the promotion effects of both Mn and Zr, to obtain a stable catalyst with a high initial activity. The structural reason for this high initial activity and stability was discussed in detail.

2 Experimental

2.1 Catalyst preparation

The Zr and Mn co-promoted catalysts were prepared by different impregnation methods.

The SiO_2 support was impregnated with an aqueous solution containing an appropriate amount of $Ni(NO_3)_2$, $Zr(NO_3)_4$ and $Mn(NO_3)_2$. After 24 h at 20 °C without stirring, the excess solvent (deionized water) was removed by heating at 80 °C in bath. Then the samples were dried at 110 ºC for 4 h and calcined at 800 ºC for 5 h in air, yielding the Ni-ZrO_X-MnO_X/SiO_2 catalyst.

Then, for the Ni-MnO_X/SiO_2 and Ni-ZrO_X/SiO_2 catalysts, the preparation details of which were the same as those reported in our previous work.[30] The SiO_2 support (20-40 mesh, 320 m^2/g) was impregnated with an aqueous solution containing an appropriate amount of $Ni(NO_3)_2$, $Zr(NO_3)_4$ or $Mn(NO_3)_2$ for 24 h at 20 °C without stirring, and then the excess solvent was removed by heating at 80 °C. After that, the samples were dried at 110 ºC for 4 h and finally calcined at 800 ºC for 5 h in air, yielding the Ni-MnO_X/SiO_2 or Ni-ZrO_X/SiO_2 catalyst. Then, the Ni-MnO_X/SiO_2 or Ni-ZrO_X/SiO_2 catalyst was impregnated with an aqueous solution containing appropriate amount of $Zr(NO_3)_4$ or $Mn(NO_3)_2$, respectively. After 24 h at 20 °C without stirring, the excess solvent was removed by heating at 80 °C. Then the samples were dried at 110 ºC for 4 h and calcined at 800 ºC for 5 h in air, yielding the Zr-promoted Ni-MnO_X/SiO_2 catalyst (ZrO_X/Ni-MnO_X/SiO_2) or the Mn-promoted Ni-ZrO_X/SiO_2 catalyst (MnO_X/Ni-ZrO_X/SiO_2), respectively.

All of the three-component catalysts have the same controlled ratio of Ni/Mn/Zr = 2/1/1 and an equal amount of Ni, while the controlled ratio of the two-component samples is Ni/Mn(or Zr) = 2/1.

2.2 Activity test

The catalytic activity test was carried out in a fixed-bed continuous flow micro-quartz-tube reactor at atmospheric pressure, which was the same as that reported in our previous work.[30] The conversions of CH_4 and CO_2, the selectivity for H_2 and CO, and the yield of products from the DRM reaction were calculated using the following equations, respectively.

$$X_{CH_4} = \frac{n_{CH_4,\ in} - n_{CH_4,\ out}}{n_{CH_4,\ in}} \times 100\%$$

$$X_{CO_2} = \frac{n_{CO_2,\ in} - n_{CO_2,\ out}}{n_{CO_2,\ in}} \times 100\%$$

$$S_{H_2} = \frac{n_{H_2}}{2n_{CH_4,\ in} - 2n_{CH_4,\ out}} \times 100\%$$

$$S_{CO} = \frac{n_{CO}}{n_{CH_4,\ in} - n_{CH_4,\ out}} \times 100\%$$

$$Y_i = X_i \times S_i \times 100\%$$

$$CO/H_2 = Y_{CO} / Y_{H_2}$$

where X_i is the conversion of *i* species (%), S_i is the selectivity for *i* species (%), Y_i is the yield of *i* species (%), and n_i is the number of moles of *i* species.

2.3 Catalyst characterization

X-ray diffraction (XRD) was performed on a DX-1000 CSC diffractometer instrument operated at 40 kV and 25 mA with a Cu Kα monochromatic X-ray radiation. The data were collected over the scattering angle range of 2θ from 10° to 80° with a step of 0.06 ° s^{-1}.

Scanning Transmission Electron Microscopy with energy dispersive spectroscopy (STEM-EDX) Mapping images were performed on an FEI company Tecnai G2 20 Twin instrument equipped with an EDX spectrometer operated at an acceleration voltage of 200 kV (recording time approx. 30 min).

The morphologies of the catalysts were examined by scanning electron microscopy (SEM, FEI Inspect F). The samples were covered with a thin film of gold to improve the conductivity.

X-ray photoelectron spectroscopy (XPS) analysis was performed on an AXIS Ultra DLD (KRATOS) spectrometer using Al Kα radiation (1486.6 eV) operated at an accelerating power of 150 W.

Temperature-programmed reduction (TPR) was carried out to determine the reduction behaviour of the catalysts, the experimental details was the same as those reported in the previous work.[30]

Temperature-programmed techniques were performed to determine the performance of the deposited carbon. The reduced catalyst was subjected to temperature-programmed heating from 60 °C to 800 °C (10 °C min^{-1}) under a dilute CH_4 atmosphere (F_{CH4} = 5 mL min^{-1} and F_{Ar} = 30 mL min^{-1}), which was designated to CH_4 temperature-programmed decomposition (CH_4-TPDe). After that, the sample was cooled in Ar flow. This was followed by either temperature-programmed hydrogenation with H_2 (H_2-TPH) or temperature-programmed oxidation with CO_2 (CO_2-TPO) and/or O_2 (O_2-TPO). Similar to the CH_4-TPDe, the sample was tested from

approximately 60 °C to 800 °C at 10 °C min^{-1} under Ar diluted CO_2, O_2 or H_2 atmosphere. The flow rate of CO_2, O_2 or H_2 was 5 mL min^{-1}, and the flow rate of Ar was 30 mL min^{-1}. The CO (m/e = 28), CO_2 (m/e = 44), CH_4 (m/e = 16), and H_2 (m/e = 2) products were recorded using a HPR-20QIC On-Line Gas Mass Spectrometer (MS).

Thermogravimetric (TG) analysis was used to monitor the amount of the carbon deposition on the spent catalysts. The experiments were performed with a sample of 15-30 mg heated from 30 °C to 800 °C at a heating rate of 10 °C min^{-1} in air flow on a SDT Q600 thermo-analyser.

Raman spectra analyses of the spent catalysts were performed on a LabRAM HR Raman Spectrometer (HORIBA Jobin Yvon) equipped with a He-Ne laser source.

3 Results and discussion

3.1 The origin of the deactivation of Ni-ZrO_X/SiO_2 catalyst in DRM

Our previous results showed that the Ni-ZrO_X/SiO_2 catalyst displayed a high initial catalytic activity for DRM. However, a monotonically decreasing of activity was not avoided within 60 h.[30] To investigate the cause of the deactivation of the Ni-ZrO_X/SiO_2 catalyst, we conducted a comparative experiment under the same reaction conditions with interval elimination of the deposited carbon (Figure 1A). The process of this experiment is the following: after every 7-12 h when the conversions of CO_2 and CH_4 clearly decreased, the feed was switched to diluted O_2 (F_{Ar} = 30 mL min^{-1}, F_{O2} = 5 mL min^{-1}) for the removal of the deposited carbon (coke elimination). That is to say, the DRM reaction was stopped, and the removal of the deposited carbon was carried out in diluted O_2. After the coke elimination, the feed was switched back to CO_2/CH_4 mixture again to perform the DRM reaction. After another 7-12 h reaction, coke elimination was performed. The system was thus fed alternatively by CO_2/CH_4 and Ar/O_2 until the 60 h activity test. It could be seen that after coke elimination, the catalytic activity of the Ni-ZrO_X/SiO_2 catalyst was well recovered (Figure 1A).

In another control experiment (Figure 1B), a small amount of O_2 was added (F_{CH4} = F_{CO2} = 30 mL min^{-1}, F_{O2} = 5 mL min^{-1}) in the DRM process compared with the DRM process (F_{CH4} = F_{CO2} = 30 mL min^{-1}). Although the introduction of O_2 will bring in a new reaction (CH_4 oxidized by O_2) in the DRM reaction in addition to elimination of the deposited carbon, the carbon deposition was effectively suppressed in this way. The Ni-based catalysts are also a promising catalysts for partial oxidation of methane reaction (POM).[31-33] It was observed that the products obtained in the presence of O_2 were the same (H_2, CO, and H_2O) as those obtained in the normal DRM whereas their distribution (the relative ratio) varied, and the O_2 was consumed completely. O_2 could react with H_2, CH_4 and deposited carbon, which results in higher ratio of CO/H_2. The CO/H_2 ratio obtained increased from 1.45 to 1.48, and the conversion of the CO_2 was descreased when the O_2 added in the DRM reaction.

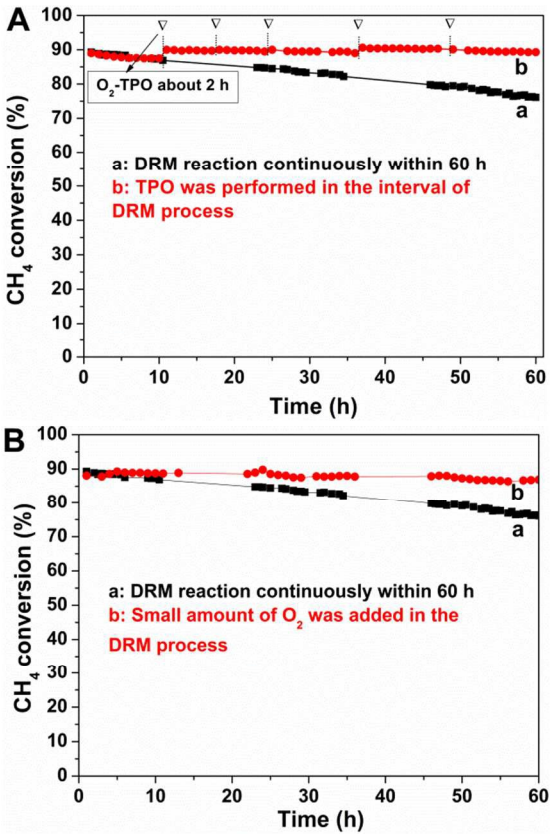

Fig. 1 The activity variation with time on stream on Ni-ZrO_X/SiO_2 catalyst at 800 °C. Conditions: F_{CH4} = F_{CO2} = 30 mL min^{-1}.

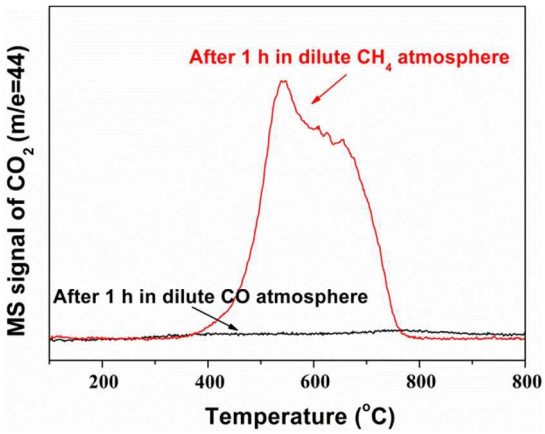

Fig. 2 O_2-TPO: CO_2 formation on Ni-ZrO_X/SiO_2 catalyst after 1 h reaction on-stream in dilute CH_4 atmosphere or CO atmosphere at 800 °C (Conditions: F_{Ar} = 30 mL min^{1}, F_{O2} = 5 mL min^{-1}).

The results showed that the Ni-ZrO_X/SiO_2 catalyst retained its good catalytic stability for the DRM reaction with O_2 added. This observation should be ascribed to the fact that the presence of O_2 could eliminate the deposited carbon in time during the reaction or prevent the formation of deposited carbon, thus preventing the Ni-ZrO_X/SiO_2 catalyst from deactivation caused by carbon deposition.

It was shown that the deactivation of the Ni-ZrO_X/SiO_2 catalyst originated from carbon deposition, whereas the deposited carbon could be eliminated to regenerate the catalyst by oxidation. Moreover, by introduction of a stronger oxidant O_2 in the reaction atmosphere, the catalyst showed high stability.

Most researchers agreed that carbon formation was the primary reason for the catalyst deactivation and proposed that the carbon deposits causing catalyst deactivation originated from CH_4 decomposition and CO disproportionation.[10,12,14,29,34-36] We further studied the origin of the carbon deposition (see Figure 2). After 1 h reaction in dilute CH_4 atmosphere (or CO atmosphere) at 800 °C, O_2-TPO (conditions: F_{Ar} = 30 mL min^{-1}, F_{O2} = 5 mL min^{-1}) had been performed, and the formation of CO_2 was detected by MS. The results showed that the main source of the carbon deposited on the Ni-ZrO_X/SiO_2 catalyst during the DRM process was from the CH_4 decomposition, and that due to CO disproportionation was negligible because there was a large amount of deposited carbon on the Ni-ZrO_X/SiO_2 catalyst after being treated in dilute CH_4 atmosphere, whereas little deposited carbon was observed on the Ni-ZrO_X/SiO_2 catalyst after being treated in dilute CO atmosphere.

3.2 Stability and activity tests of Zr and Mn co-promoted catalysts

The activity of Ni-MnO_X/SiO_2 and Ni-ZrO_X/SiO_2 catalysts was shown in our previous work.[30] The Ni-ZrO_X/SiO_2 catalyst showed relatively high initial activity (CH_4 conversion was 89.3% at 1 h), but it decreased monotonically with time on stream. Whereas the Ni-MnO_X/SiO_2 catalyst showed stable activity within 60 h tested although the initial activity (CH_4 conversion was 77.8% at 1 h) over it was lower than that over Ni-ZrO_X/SiO_2 catalyst. The enhancement of the initial catalytic activity of Mn was weaker than that of Zr.

Figure 3 shows the variation in CH_4 and CO_2 conversions with time on stream over each of the three Zr and Mn co-promoted catalysts prepared by different impregnation methods. The CO_2 conversions (Figure 3B) were all higher than those of methane (Figure 3A) due to the presence of the reverse water gas shift reaction. In agreement with this, the CO/H_2 ratios were all greater than 1. It was interesting to discover that all the three catalysts showed quite good stability during the 60-h DRM reaction at 800 °C.

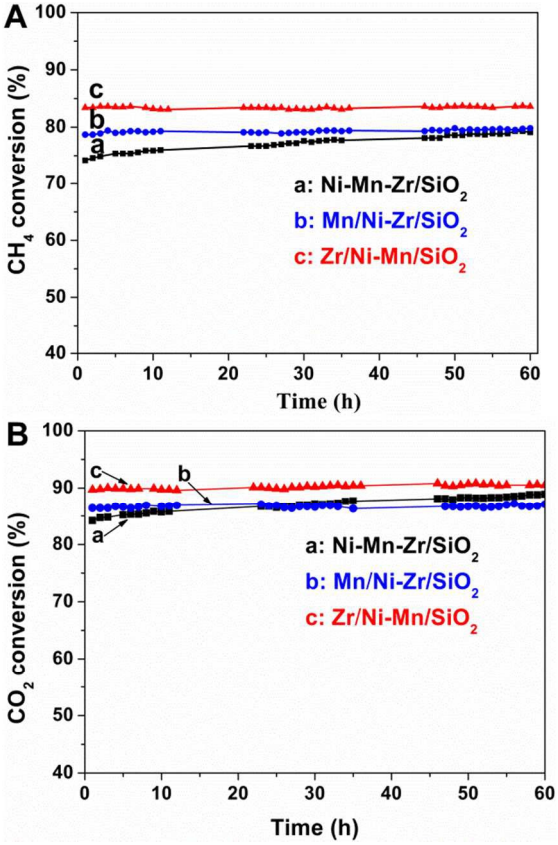

Fig. 3 The activity variation with time on stream on different Zr and Mn co-promoted catalysts during the DRM reaction at 800 °C.

It was indicated in our previous work that the Mn promoter enhanced the anti-carbon deposition performance of the Ni/SiO_2 catalyst and thus maintained a good stability, whereas the Zr promoter exhibited a great ability to enhance the initial catalytic activity of the Ni/SiO_2.[30] The above data suggested that all the three Mn and Zr co-promoted catalysts avoided the disadvantages of deactivation caused by the Zr promoter alone and inherited the advantage of Mn to enhance the catalytic stability. It was also interesting to find that Ni-MnO_X-ZrO_X/SiO_2 showed the lowest catalytic activity, which was even lower than that of the Ni-MnO_X/SiO_2 catalyst. Besides, during our 60 h activity test, CH_4 conversions showed slight increasing trends on Ni-MnO_X-ZrO_X/SiO_2 catalyst, which was similar to the activity variation trends of the Ni-MnO_X/SiO_2 catalyst. The conversion of CO_2 also showed the same variation trends. Thus, although the CO_2 conversion on MnO_X/Ni-ZrO_X/SiO_2 catalyst was higher than that of Ni-MnO_X-ZrO_X/SiO_2 catalyst at 1 h, it showed the reverse relationship after 30 h test. MnO_X/Ni-ZrO_X/SiO_2 exhibited relatively higher catalytic activity than Ni-ZrO_X-MnO_X/SiO_2, but the initial conversion of CH_4 on MnO_X/Ni-ZrO_X/SiO_2 was similar to that on Ni-MnO_X/SiO_2. The initial activity of the ZrO_X/Ni-MnO_X/SiO_2 catalyst was lower than that of the Ni-ZrO_X/SiO_2, but higher than that of Ni-MnO_X/SiO_2 catalyst. The initial catalytic activity varied by the order of Ni-ZrO_X/SiO_2 > ZrO_X/Ni-MnO_X/SiO_2 > Ni-MnO_X/SiO_2 ≈ MnO_X/Ni-ZrO_X/SiO_2 >

Ni-ZrO_X-MnO_X/SiO_2. These facts might indicate that Mn promoter could result in the relatively lower initial activity of the ZrO_X/Ni-MnO_X/SiO_2 catalyst compared to that of the Ni-ZrO_X/SiO_2 catalyst, although the initial activity of the Ni-MnO_X/SiO_2 catalyst was higher than that of the un-promoted Ni/SiO_2 catalyst. The addition of Mn promoter may lead to the results that the Zr promoter cannot give the full function of initial activity improvement (compared with the Ni-ZrO_X/SiO_2 catalyst). Nevertheless, the initial catalytic activity was higher than that of the Ni-MnO_X/SiO_2 catalyst with a much higher stability than that of the Ni-ZrO_X/SiO_2 catalyst. Therefore, it could be deduced that the ZrO_X/Ni-MnO_X/SiO_2 catalyst inherited the advantages of both the Ni-MnO_X/SiO_2 (high stability) and Ni-ZrO_X/SiO_2 (high initial activity) catalysts. Moreover, the initial (at 1 h) conversions of CH_4 and CO_2 on ZrO_X/Ni-MnO_X/SiO_2 catalyst at 600 °C were 31.9% and 38.7%, respectively. Besides, the ZrO_X/Ni-MnO_X/SiO_2 catalyst showed good stability at 600 °C, the conversions of CH_4 and CO_2 on ZrO_X/Ni-MnO_X/SiO_2 catalyst at 10 h were 32.0% and 38.5% respectively.

3.3 Structural characterization of the catalysts

XRD profiles showed that (Figure S1) after H_2 reduction at 800 °C, nickel species existed mainly in the form of metallic Ni. The Ni, Mn, and Zr distribution mapping of EDX (energy-dispersive X-ray spectroscopy) analysis and HAADF (high-angel annular dark field detector) images for the reduced catalysts are illustrated in Figure 4. The elemental maps of Ni, Mn and Zr showed in the red box section in HAADF images, and the yellow box in HAADF images was used to correct the drift when the mapping EDX images were collecting. The turquoise, fuchsia and green points (or areas) represented the signals of the elements Ni, Mn and Zr, respectively. As shown in Figure 4, the dispersion of these three metals (Ni, Mn and Zr) on the Mn and Zr co-promoted catalysts was clearly influenced by the preparation method. The dispersion of both Ni and Zr were poor on Ni-MnO_X-ZrO_X/SiO_2 catalyst compared to that of either MnO_X/Ni-ZrO_X/SiO_2 or ZrO_X/Ni-MnO_X/SiO_2, and the dispersion of the Mn species was also lower than that on ZrO_X/Ni-MnO_X/SiO_2. For MnO_X/Ni-ZrO_X/SiO_2, the dispersion of the Ni species was better than that of the Ni-MnO_X-ZrO_X/SiO_2, but the dispersion of Mn was relatively poor (clearly gathered). The ZrO_X/Ni-MnO_X/SiO_2 catalyst ensured a superior dispersion of all the three metal (Ni, Mn and Zr) species. The XPS (Table S1) results showed that the surface Ni content on Ni-MnO_X-ZrO_X/SiO_2, MnO_X/Ni-ZrO_X/SiO_2 and ZrO_X/Ni-MnO_X/SiO_2 was 37.3%, 39.4% and 46.2%, respectively. The results of the Ni surface exposure measured from CO chemisorptions (Table S2) showed that among the three Mn and Zr co-promoted catalysts, the ZrO_X/Ni-MnO_X/SiO_2 catalyst exhibited the highest Ni dispersion on the catalyst surface. This result was in agreement with the results of XPS. Despite all samples having the same controlled amount of Ni, the ZrO_X/Ni-MnO_X/SiO_2 possessed a high surface Ni species content. These results were in line with the relatively high activity and stability of ZrO_X/Ni-MnO_X/SiO_2 catalyst .

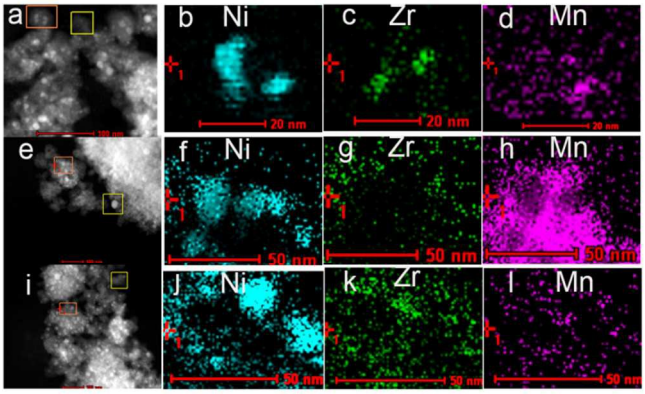

Fig. 4 Effect HAADF images and mapping EDX analysis of Ni, Zr and Mn particles for the reduced Zr and Mn co-promoted catalysts. a-d) Ni-MnO_X-ZrO_X/SiO_2, e-h) MnO_X/Ni-ZrO_X/SiO_2 and i-l) ZrO_X/Ni-MnO_X/SiO_2 catalysts.

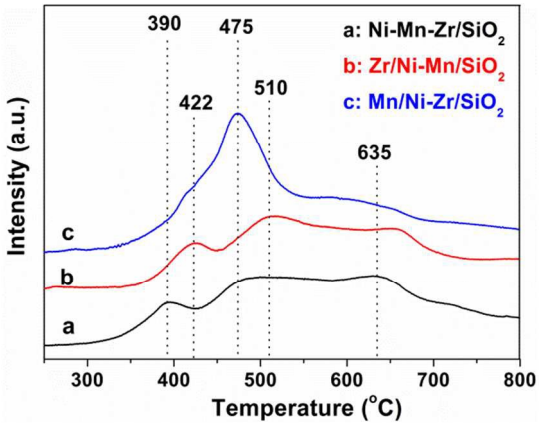

Fig. 5 TPR profiles of different Zr and Mn co-promoted catalysts.

The TPR profiles of the three Mn and Zr co-promoted catalysts are displayed in Figure 5. The Mn and Zr co-promoted catalysts kept lots of the reduction performance of their precursor. Comparing with the previous TPR results of the Ni/SiO_2, MnO_X/SiO_2, ZrO_X/SiO_2, Ni-MnO_X/SiO_2 and Ni-ZrO_X/SiO_2, the ZrO_X/Ni-MnO_X/SiO_2 catalyst exhibited reduction patterns similar to that of Ni-MnO_X/SiO_2 catalyst, and the broad reduction peaks of which reflected the complex reduction of MnO_x and some NiO species.[30] Whereas MnO_X/Ni-ZrO_X/SiO_2 catalyst exhibited reduction patterns similar to that of the Ni-ZrO_X/SiO_2 catalyst, and a main peak was observed at approximately 475 °C, while two shoulders were observed at approximately 400 and 600 °C. The shoulders could probably be due to the reduction of MnO_x species, which is consistent with the TPR profile of MnO_X/SiO_2.[30] The major peak (at approximately 475 °C) was tentatively assigned to the reduction of the NiO species which possess the medium strong interaction with SiO_2.[30] Moreover, according to a previous study,[30] the introduction of Mn promoter may weaken the reducibility of the Ni/SiO_2 catalyst. The reduction peaks of ZrO_X/Ni-

MnO_X/SiO_2 were all shifted to a higher temperature compared to those of the Ni-ZrO_X-MnO_X/SiO_2 due to stronger interactions between the metallic oxides and support. This observation indicated that the impregnation sequence of the promoters played an important role in the reducibility of the NiO and MnO_x species.

Li et al.[4], Yao et al.[37] and Zhang et al.[38] reported the relationship between confinement effect, catalytic activity and stability. They suggested that the confinement effect contributed to the dispersion of the central active metal, resulting in the high stability and/or high activity. Thus, we deduced that the Mn species dispersed well on the surface of the catalyst and then made a better dispersion of Ni species. Mn might act as an obstacle for sintering, which plays an important role in maintaining strong stability, and the introduction of Zr may form a special interaction (including electric effect) with the Ni species, mainly contributing to the high initial activity.

3.4 Characterization of the deposited carbon

The TG profiles of the used catalysts after 60 h of DRM reaction at 800 °C are presented in Figure 6. The weight loss below 110 °C was due to moisture.[27] Thus, the weight loss caused by eliminating the deposited carbon was estimated at above 110 °C to exclude the interference of moisture. It was observed that the deposited carbon on the Zr and Mn co-promoted catalysts was quite low (the weight losses were all below 1.0 %).

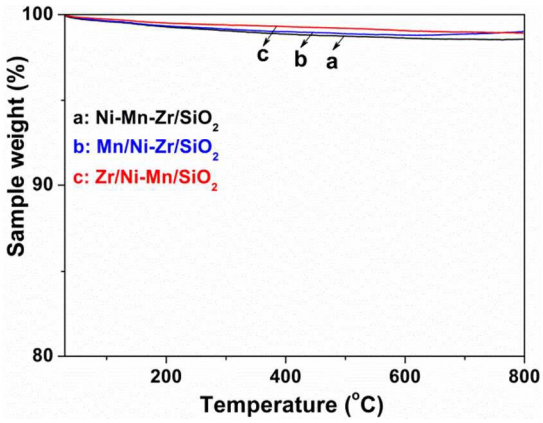

Fig. 6 TG profiles of different Zr and Mn co-promoted catalysts after 60 h of reaction at 800 °C.

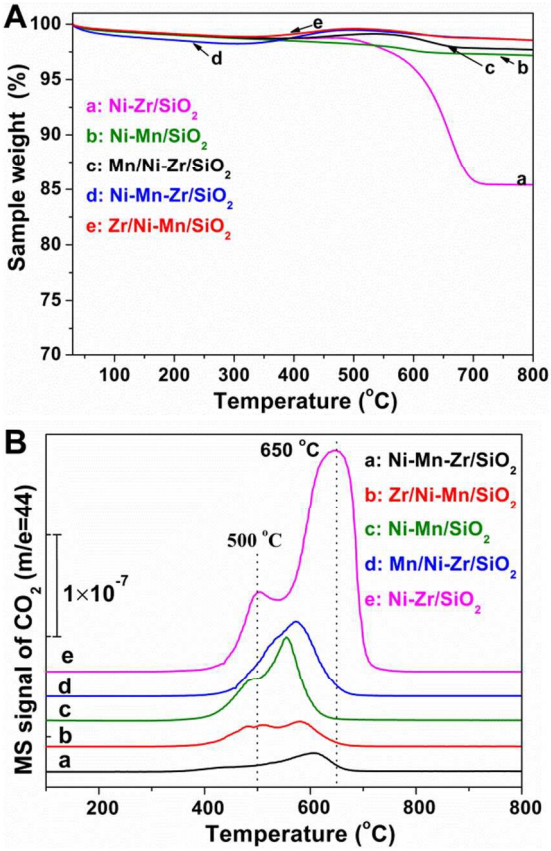

Fig. 7 A) TG and B) direct O_2-TPO profiles of different catalysts after CH_4-TPDe.

The TG profiles of the catalysts after CH_4-TPDe are presented in Figure 7A. The weight gain arising from Ni oxidation was observed at approximately 350-400 °C.[39] Considering the same control amount of Ni, the weight gain by oxidation of Ni was regarded as the same. The total amount of carbon deposition over these samples was decreased in the following sequence: Ni-ZrO_X/SiO_2 (14.1%) > Ni-MnO_X/SiO_2 (2.1%) > MnO_X/Ni-ZrO_X/SiO_2 (1.7%) > ZrO_X/Ni-MnO_X/SiO_2 (1.1%) > Ni-MnO_X-ZrO_X/SiO_2 (1.0%). It can be seen that the carbon formation via CH_4 decomposition on the Ni-ZrO_X/SiO_2 catalyst was effectively suppressed with the addition of the Mn promoter. As the above data quantified by TG could not separate the amount of weight gain by the oxidation of Ni, the TPO by MS was implemented at the same time. After CH_4-TPDe, the direct O_2-TPO was performed to study the reactivity of the deposited carbon formed on the catalysts, as shown in Figure 7B. The O_2-TPO results indicated that there were different types of carbon deposition that possessed different reactivity to O_2 at different temperatures. As the amount of the CO_2 formation (the intensity of the CO_2 formation peak) is proportional to the amount of the carbon deposition, the order of the amount of the deposited carbon was as follows according to the amount of CO_2 released: Ni-MnO_X-ZrO_X/SiO_2 < ZrO_X/Ni-MnO_X/SiO_2 < Ni-MnO_X/SiO_2 ≈ MnO_X/Ni-ZrO_X/SiO_2 < Ni-ZrO_X/SiO_2. For the Ni-ZrO_X/SiO_2 sample, there were two main regions for CO_2 formation with maxima at approximately 500 and 650 °C,

which showed the different activities of different types of deposited carbon (relatively active and inert carbon). In addition to the low amount of carbon deposition, the CO_2 formation peaks shifted to lower temperatures for all of the Mn-added samples. Almost all of the deposited carbon could be eliminated below 600 °C in dilute O_2 atmosphere on the Mn-added catalysts. For the ZrO_X/Ni-MnO_X/SiO_2 catalyst, three regions of CO_2 formation, with maxima at approximately 475, 510 and 580 °C, were identified. Thus, it could be seen that the ZrO_X/Ni-MnO_X/SiO_2 catalyst facilitated the elimination of the deposited carbon from CH_4 decomposition.

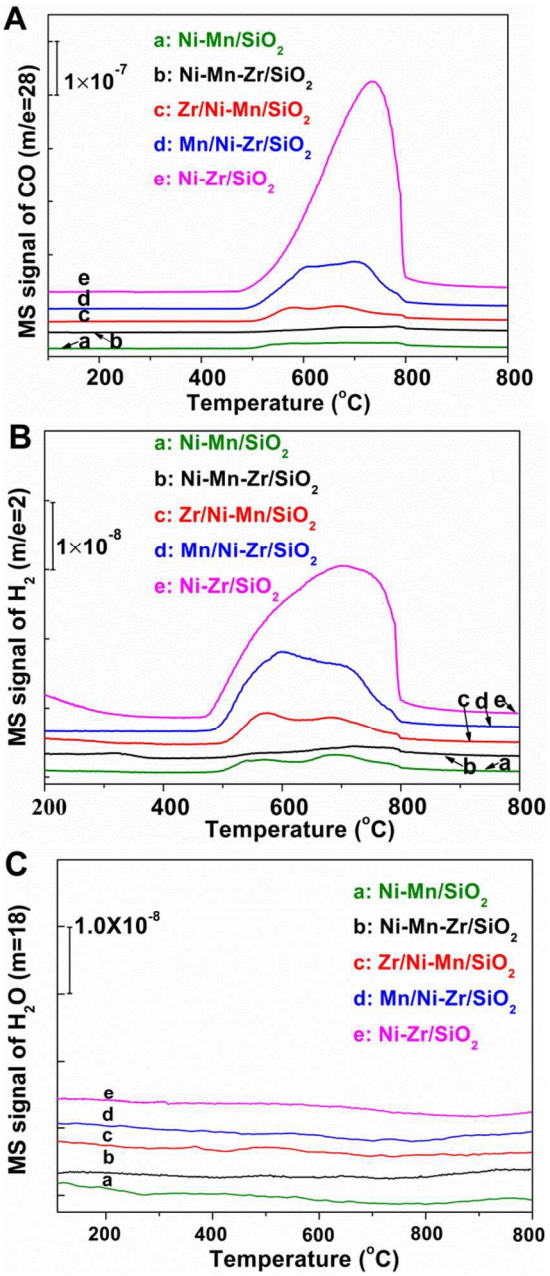

Fig. 8 The A) CO, B) H_2 and C) H_2O formation profiles of different catalysts during CO_2-TPO.

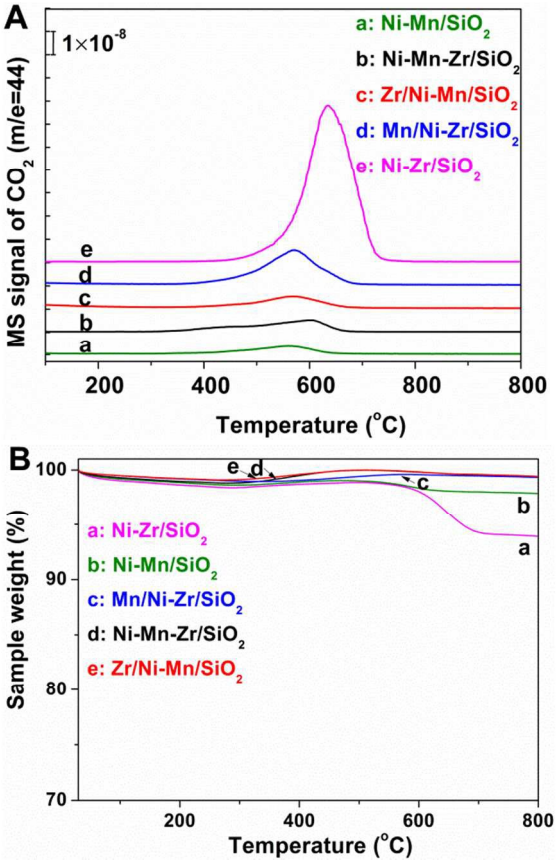

Fig. 9 A) O_2-TPO and B) TG profiles of different catalysts after CO_2-TPO.

The subsequent CO_2-TPO after CH_4-TPDe was performed to eliminate the CO_2-oxidizable carbon because the deposited carbon possessed different reactivity and performance (Figure 8). Because the intensity of the CO formation peak is proportional to the amount of the carbon deposition, the order of the amount of CO_2-oxidizable carbon deposition on these catalysts was Ni-ZrO_X/SiO_2 > MnO_X/Ni-ZrO_X/SiO_2 > ZrO_X/Ni-MnO_X/SiO_2 > Ni-MnO_X/SiO_2 > Ni-MnO_X-ZrO_X/SiO_2 (Figure 8A). This suggested that the amount of the CO_2-oxidizable carbon on ZrO_X/Ni-MnO_X/SiO_2 was larger than that on the Ni-MnO_X/SiO_2 catalyst while the total amount of the carbon deposition (from Figure 7 TG and O_2-TPO profiles) on the ZrO_X/Ni-MnO_X/SiO_2 catalyst was lower than that on Ni-MnO_X/SiO_2 catalyst. This also suggested that the carbon deposited on the ZrO_X/Ni-MnO_X/SiO_2 catalyst possessed higher reactivity than that on Ni-MnO_X/SiO_2 catalyst.

H_2 was observed during the CO_2-TPO process (Figure 8B) at the same time. It was thought to come from polymer cokes that can be gasified (including the pyrolysis of polymeric coke producing H_2) under relatively mild conditions and did not accumulate on the active sites.[22] It could be deduced that the carbon deposited on the catalyst via CH_4 decomposition produced CH_x forms of carbon in addition to the general carbon deposition (mainly consisting of C-C). As shown in Figure 8C, no MS signal changes were detected for H_2O (m/e = 18)

indicating the absence of H_2O formation. The O atom of CO_2 will react with the C atom of the CH_x to form CO and simultaneously release H_2 instead of forming H_2O. The order of the amount of H_2 formed on those catalysts was Ni-MnO_X-ZrO_X/SiO_2 < Ni-MnO_X/SiO_2 < ZrO_X/Ni-MnO_X/SiO_2 < MnO_X/Ni-ZrO_X/SiO_2 < Ni-ZrO_X/SiO_2. This affirmed again that the total amount of the carbon deposition (from Figure 7 O_2-TPO and TG profiles) on the ZrO_X/Ni-MnO_X/SiO_2 catalyst was smaller than that on the Ni-MnO_X/SiO_2 catalyst, while a larger amount of polymeric carbon capable of being gasified easily formed on the ZrO_X/Ni-MnO_X/SiO_2 catalyst than on the Ni-MnO_X/SiO_2 catalyst. This indicated that the ZrO_X/Ni-MnO_X/SiO_2 catalyst was better at restraining carbon deposition, and at the same time, the amount of deposited carbon in the form of CH_x was greater than that on the Ni-MnO_X/SiO_2 catalyst.

After CO_2-TPO, O_2-TPO was employed to determine the portion of the coke that was resistant to CO_2 (Figure 9A). It showed that the deposited carbon which could be eliminated directly by O_2 below 500 °C (Figure 7B) was mostly removed by CO_2 during the CO_2-TPO process. The deposited carbon that could be eliminated by O_2 above 500 °C was difficult to be eliminated by CO_2, especially on the Ni-ZrO_X/SiO_2 catalyst. It can be seen that the ability of CO_2 to eliminate the deposited carbon was much stronger than that of H_2 given the results in Figure S2, because there were much larger amounts of carbon deposition resistant to H_2 than to CO_2.

It was shown that the introduction of Mn clearly inhibited the carbon deposition, whereas there was a large amount of deposited carbon on the Ni-ZrO_X/SiO_2 catalyst. Although some of the deposited carbon on Ni-ZrO_X/SiO_2 catalyst was CO_2-oxidizable, there was still a certain amount of deposited carbon that is not reactive with CO_2. The inactive carbon (not reactive with CO_2) deposition may be the main reason for the deactivation of the Ni-ZrO_X/SiO_2 catalyst.

It was indicated that ZrO_X/Ni-MnO_X/SiO_2 catalyst not only inhibited the carbon deposition, but also changed the form of deposited carbon, and then accelerated the elimination of the deposited carbon, which played an important role in the stability of the catalyst. As a larger amount of CH_x species was formed via CH_4 decomposition on the ZrO_X/Ni-MnO_X/SiO_2 catalyst than on the Ni-Mn/SiO_2 catalyst, and the CH_x species could be gasified by CO_2 to release H_2 and CO instead of H_2O. The ZrO_X/Ni-MnO_X/SiO_2 catalyst consumed more CO_2 to eliminate the CH_x species, which facilitated the DRM reaction. This led to higher catalytic activity.

Raman spectroscopy has been extensively used to probe the structure and the crystallite size of coke on reforming catalysts.[39-42] Figure 10 displays the Raman spectra of catalysts after CH_4-TPDe, CO_2-TPO (after CH_4-TPDe), O_2-TPO (after CO_2-TPO), and 60 h of DRM reaction.

For the samples used after CH_4-TPDe (Figure 10A), all recorded Raman spectra showed four major bands at approximately 1325 cm^{-1} (D band), 1578 cm^{-1} (G band), 1604 cm^{-1} (D′ band) and 2649 cm^{-1} (G′ band), respectively. The D band, also known as the disorder-induced band, was mainly due to structural imperfections, which exist in defective polycrystalline graphite and other carbon materials, whereas the G band was assigned to 'in plane' displacement of the carbons strongly coupled in the hexagonal sheet of the graphite (well-ordered graphitic carbon that arose from the in-plane carbon–carbon stretching vibrations of pairs of sp^2 carbons).[40-43] The D′ band, a shoulder peak in the G band, is also associated with the presence of defects in graphite and other carbonaceous species.[40,42] The G′ band appearing at approximately twice the frequency of the D band as its second harmonic is independent.[42-43] The ratio of the D and G bands of integrated intensities (I_D/I_G) of carbons on Ni-ZrO_X/SiO_2, Ni-MnO_X/SiO_2, Ni-MnO_X-ZrO_X/SiO_2, MnO_X/Ni-ZrO_X/SiO_2 and ZrO_X/Ni-MnO_X/SiO_2 catalysts were 1.6, 1.3, 1.0, 0.8 and 1.1, respectively.

For the catalysts treated by sequential CH_4-TPDe and CO_2-TPO, both the D band and the G band were still observed (Figure 10B), and the ratio of the D and G bands of integrated intensities (I_D/I_G) of carbons on Ni-ZrO_X/SiO_2, Ni-MnO_X/SiO_2, Ni-MnO_X-ZrO_X/SiO_2, MnO_X/Ni-ZrO_X/SiO_2 and ZrO_X/Ni-MnO_X/SiO_2 catalysts were 2.0, 1.4, 0.5, 1.4 and 1.0, respectively. Decreased intensities of the Raman peaks were observed, especially for the ZrO_X/Ni-MnO_X/SiO_2 catalyst. This observation suggested that the carbon deposited on the catalysts after CH_4-TPDe were partly eliminated by CO_2, which was in agreement with the TG and TPO results. As the ratios of the D and G bands of integrated intensities were altered, the structures of the deposited carbon were changed by CO_2-TPO.

For the catalysts after sequential CH_4-TPDe, CO_2-TPO and O_2-TPO, neither the D band nor the G band were observed (Figure 10C). This indicated that the deposited carbon was eliminated completely or that the amount of carbon deposition remaining on these samples was too small to be observed. For the three Zr and Mn co-promoted catalysts after 60 h of reaction (Figure 10D), the Raman spectra were similar to those of catalysts after O_2-TPO, that is, neither the D band nor the G band was observed. This may be caused by the fact that the amount of deposited carbon that shows Raman scattering on those catalysts was too low. These results were also in agreement with the TG results (Figure 6), that is, there was a very low amount of carbon deposited on the Zr and Mn co-promoted catalysts.

Some researchers reported that the formation of deposited carbon in the form of carbon nanotubes, nanofibers and whiskers like could be helpful for keeping the stability, in spite of the increasing amount of carbon deposited on the catalysts.[24, 44]

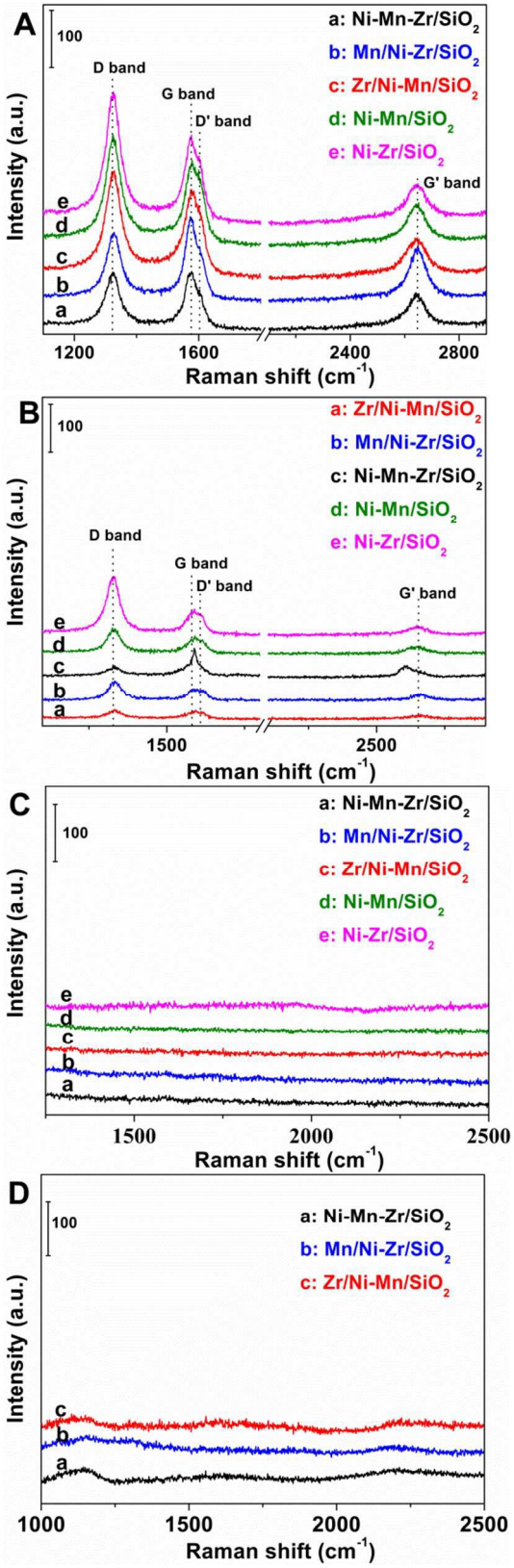

Fig. 10 Raman spectra of carbon deposition over different catalysts after A) CH_4-TPDe, B) CO_2-TPO after CH_4-TPDe, C) O_2-TPO after CO_2-TPO, and D) after 60 h reaction at 800 °C.

SEM images of the catalysts after CH_4-TPDe, CO_2-TPO and subsequent O_2-TPO were shown in the supporting information section (Figure S3). After CH_4-TPDe, a small amount of nanotube like deposited carbon on Ni-ZrO_X/SiO_2 catalyst was observed, whereas on other Mn-promoted catalysts no obvious nanotube like deposited carbon was observed. Thus, the formation of deposited carbon in the form of carbon nanotubes or nanofibers may be not the main reason for the high stability. The high stability may be caused by the low amount of the carbon formation on the Mn-promoted catalysts.

4 Conclusions

The main reason for deactivation of the Ni-ZrO_X/SiO_2 catalyst was CO_2-unoxidizable carbon deposition via CH_4 decomposition rather than CO disproportionation, despited the high initial activity. This process could be effectively suppressed by the addition of the second promoter, Mn. The preparation method contributed significantly to the structure and catalytic activity of the Zr and Mn co-promoted catalysts. The ZrO_X/Ni-MnO_X/SiO_2 catalyst ensured a superior dispersion of all the three metal (Ni, Mn and Zr) species as well as strong interactions between the metallic oxides and support. On ZrO_X/Ni-MnO_X/SiO_2 catalyst, in addition to high ability of inhibiting carbon deposition, the form of deposited carbon was also changed, which accelerated the elimination of the deposited carbon. The dispersion of the metals, the interaction between Ni and Zr or Mn, and the structure of the catalyst could play an important role in the types of the deposited carbon. CH_x species formed via CH_4 decomposition on the ZrO_X/Ni-MnO_X/SiO_2 catalyst could be gasified by CO_2 to release H_2 and CO instead of H_2O. Thus, the ZrO_X/Ni-MnO_X/SiO_2 catalyst showed both high initial activity and excellent stability.

Acknowledgements

The authors are grateful for financial support from the Ministry of Science and Technology (Nos. 2012BAC20B10) and the National Natural Science Foundation of China (Nos. 20976109 and 21321061). The characterization of the catalysts by the Analytical and Testing Centre of Sichuan University was also appreciated.

Notes and references

Key Laboratory of Green Chemistry and Technology, Ministry of Education, College of Chemistry, Sichuan University, Chengdu, Sichuan, 610064, China. Tel: +86-28-85411105; Fax: +86-28-85411105; E-mail: C. Hu: changweihu@scu.edu.cn
* The author was corresponding authors.

1 L. Mo, K. K. M. Leong and S. Kawi, *Catal. Sci. & Technol.*, 2014, **4**, 2107.

2 J. L. Ewbank, L. Kovarik, C. C. Kenvin and C. Sievers, *Green Chem.*, 2014, **16**, 885-896.
3 C. S. Chen, S. J. Feng, S. Ran, D. C. Zhu, W. Liu and H. J. Bouwmeester, *Angew. Chem. Int. Edit.*, 2003, **42**, 5196-5198.
4 Z. Li, L. Mo, Y. Kathiraser and S. Kawi, *ACS Catal.*, 2014, **4**, 1526-1536.
5 E. Baktash, P. Littlewood, J. Pfrommer, R. Schomäcker and M. Driess, A. Thomas, *ChemCatChem*, 2015, **7**, 1280-1284.
6 R.A. Periana, O. Mironov, D. Taube, G. Bhalla and C.J. Jones, *Science*, 2003, **301**, 814-818.
7 F. J. Keil, *Nat. Chem*. 2013, **5**, 91-92.
8 P. Tang, Q. Zhu, Z. Wu and D. Ma, *Energ. Environ. Sci*. 2014, **7**, 2580-2592.
9 D. Baudouin, K. C. Szeto, P. Laurent, A. De Mallmann, B. Fenet, L. Veyre, U. Rodemerck, C. Coperet and C. Thieuleux, *J. Am. Chem. Soc*., 2012, **134**, 20624-20627.
10 Z. Li, Y. Kathiraser and S. Kawi, *ChemCatChem*, 2015, **7**, 160-168.
11 H. Düdder, K. Kähler, B. Krause, K. Mette, S. Kühl, M. Behrens, V. Scherer and M. Muhler, *Catal. Sci. Technol*., 2014, **4**, 3317-3328.
12 M.-S. Fan, A.Z. Abdullah and S. Bhatia, *Appl. Catal. B*, 2010, **100**, 365-377.
13 D. Baudouin, U. Rodemerck, F. Krumeich, A.d. Mallmann, K. C. Szeto, H. Ménard, L. Veyre, J.-P. Candy, P.B. Webb, C. Thieuleux and C. Copéret, *J. Catal*., 2013, **297**, 27-34.
14 R. Pereñiguez, V. M. Gonzalez-delaCruz, A. Caballero and J. P. Holgado, *Appl. Catal. B*, 2012, **123-124**, 324-332.
15 A. Pechimuthu, K. K. Pant and S. C. Dhingra, *Ind. Eng. Chem. Res*., 2007, **46**, 1731-1736.
16 A. G. Bhavani, W. Y. Kim, J. Y. Kim and J. S. Lee, *Appl. Catal. A*, 2013, **450**, 63-72.
17 Z. Hou, J. Gao, J. Guo, D. Liang, H. Lou and X. Zheng, *J. Catal*., 2007, **250**, 331-341.
18 Z. Li, Y. Kathiraser, J. Ashok, U. Oemar and S. Kawi, *Langmuir*, 2014, **30**, 14694-14705.H
19 M. Broda, A. M. Kierzkowska, D. Baudouin, Q. Imtiaz, C. Copéret and C. R. Müller, *ACS Catal*., 2012, **2**, 1635-1646.
20 V. M. Gonzalez-Delacruz, R. Pereñiguez, F. Ternero, J. P. Holgado and A. Caballero, *ACS Catal*., 2011,**1**, 82-88.
21 A. Pietraszek, B. Koubaissy, A.-C. Roger and A. Kiennemann, *Catal. Today* 2011, **176**, 267-271.
22 J. Guo, H. Lou and X. Zheng, *Carbon*, 2007,**45**, 1314-1321.
23 J. Ni, L. Chen, J. Lin, M. K. Schreyer, Z. Wang and S. Kawi, *Int. J. Hydrogen Energy*, 2013, **38**, 13631-13642.
24 J. Ni, L. Chen, J. Lin, M. K. Schreyer, Z. Wang and S. Kawi, *Int. J. Hydrogen Energy*, 2013, **38**, 13631-13642.
25 K. Sutthiumporn, T. Maneerung, Y. Kathiraser and S. Kawi, *Int. J. Hydrogen Energy*, 2012, **37**, 11195-11207.
26 Y. Ma, X. Wang, X. You, J. Liu, J. Tian, X. Xu, H. Peng, W. Liu, C. Li, W. Zhou, P. Yuan and X. Chen, *ChemCatChem*, 2014, **6**, 3366-3376.
27 D. Liu, X. Y. Quek, W. N. E. Cheo, R. Lau, A. Borgna and Y. Yang, *J. Catal*., 2009, **266**, 380-390.
28 C. Fernández, N. Miranda, X. García, P. Eloy, P. Ruiz, A. Gordon and R. Jiménez, *Appl. Catal. B*, 2014, **156-157**, 202-212.
29 S.-H. Seok, S.H. Han and J.S. Lee, *Appl. Catal. A*, 2001, **215**, 31-38.
30 L. Yao, J. Zhu, X. Peng, D. Tong and C. Hu, *Int. J. Hydrogen Energy*, 2013, **38**, 7268-7279.
31 C. Ding, G. Ai, K. Zhang, Q. Yuan, Y. Han, X. Ma, J. Wang, S. Liu, *Int. J. Hydrogen Energy*, 2015, **40**, 6835-6843.
32 A.S. Larimi, S.M. Alavi, Fuel 2012, **102**, 366-371.
33 G. Pantaleo, V. La Parola, F. Deganello, P. Calatozzo, R. Bal, A.M. Venezia, *Appl. Catal. B*, 2015, **164**, 135-143.
34 S. Zeng, X. Zhang, X. Fu, L. Zhang, H. Su and H. Pan, Appl. Catal. B, 2013, **136-137**, 308-316.
35 K. Nagaoka, K. Seshan, K.-i. Aika and J. A. Lercher, *J. Catal*., 2001, **197**, 34-42..
36 M. Khajenoori, M. Rezaei and F. Meshkani, *J. Ind. Eng. Chem*., 2015, **21**, 717-722.
37 L. H. Yao, Y. X. Li, J. Zhao, W. J. Ji and C. T. Au, *Cataly. Today*, 2010, **158**, 401-408.
38 X. Zhang, Q. Zhang, N. Tsubaki, Y. Tan and Y. Han, *Fuel*, 2015, **147**, 243-252.
39 J. Zhu, X. Peng, L. Yao, J. Shen, D. Tong and C. Hu, *Int. J. Hydrogen Energy*, 2011, **36**, 7094-7104.
40 S. Zhang, S. Muratsugu, N. Ishiguro and M. Tada, *ACS Catal*., 2013, **21**, 1855-1864.
41 M. A. Pimenta, G. Dresselhaus, M. S. Dresselhaus and L. G. Canc¸ado, *Phys. Chem. Chem. Phys*., 2007, **9**, 1276-1291.
42 E. Barros, N. Demir, A. Souza Filho, J. Mendes Filho, A. Jorio, G. Dresselhaus and M. Dresselhaus, *Phys. Rev. B*, 2005, **71**, 165422.
43 D. Liu, R. Lau, A. Borgna and Y. Yang, *Appl. Catal. A*, 2009, **158**, 110-118.
44 T. Maneerung, K. Hidajat and S. Kawi, *Cataly. Today*, 2011, **171**, 24-25.

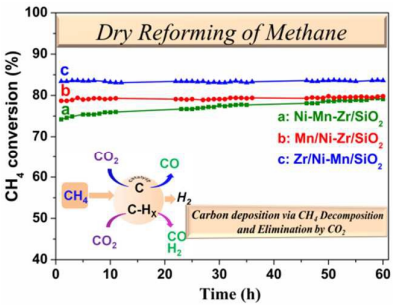

A ZrO_X/Ni-MnO_X/SiO_2 catalyst with both high activity and stability was obtained. Most of the deposited carbon was CO_2-oxidizable with the release of CO and H_2.